Structure
Article

Three-Dimensional Visualization of Gammaherpesvirus Life Cycle in Host Cells by Electron Tomography

Li Peng,[1] Sergey Ryazantsev,[2,3] Ren Sun,[2,4] and Z. Hong Zhou[1,2,*]
[1]Department of Microbiology, Immunology, and Molecular Genetics
[2]California NanoSystem Institute
[3]Department of Biological Chemistry
[4]Department of Molecular and Medical Pharmacology
University of California, Los Angeles, Los Angeles, CA 90095, USA
*Correspondence: hong.zhou@ucla.edu
DOI 10.1016/j.str.2009.10.017

SUMMARY

Gammaherpesviruses are etiologically associated with human tumors. A three-dimensional (3D) examination of their life cycle in the host is lacking, significantly limiting our understanding of the structural and molecular basis of virus-host interactions. Here, we report the first 3D visualization of key stages of the murine gammaherpesvirus 68 life cycle in NIH 3T3 cells, including viral attachment, entry, assembly, and egress, by dual-axis electron tomography. In particular, we revealed the transient processes of incoming capsids injecting viral DNA through nuclear pore complexes and nascent DNA being packaged into progeny capsids in vivo as a spool coaxial with the putative portal vertex. We discovered that intranuclear invagination of both nuclear membranes is involved in nuclear egress of herpesvirus capsids. Taken together, our results provide the structural basis for a detailed mechanistic description of gammaherpesvirus life cycle and also demonstrate the advantage of electron tomography in dissecting complex cellular processes of viral infection.

INTRODUCTION

The *Herpesviridae* is a large family of DNA viruses, including eight known types of human herpesviruses. These viruses cause many diseases, ranging from relatively mild sicknesses such as cold sores, to life-threatening tumors (reviewed by Arvin et al., 2007; Pellett and Roizman, 2007). Gammaherpesviruses form one of the three subfamilies (alpha, beta, and gamma) of the *Herpesviridae*. They are characterized by their cellular tropism for lymphocytes and are distinct from alpha and betaherpesviruses in molecular phylogenetic analyses (Ganem, 2007; Rickinson and Kieff, 2007). To date, two human gammaherpesviruses, Epstein-Barr virus (EBV) and Kaposi's sarcoma-associated herpesvirus (KSHV), are known, both of which are associated with human tumors.

Structural information about herpesviruses and their interactions with host cells is an essential part of our understanding of herpesvirus infection and spread. So far, most structural and morphogenetic studies of herpesviruses have been carried out using alphaherpesviruses, such as herpes simplex virus (HSV) and pseudorabies virus (PRV) (reviewed in Mettenleiter, 2002, 2004; Mettenleiter et al., 2006). There are fewer structural studies on gammaherpesvirus infections (Akula et al., 2003; Greenspan et al., 1989; Miller and Hutt-Fletcher, 1992; Orenstein et al., 1997), possibly due to the lack of efficient cell culture system, which show features of morphogenesis that are shared across the *Herpesviridae*. The studies cited above use conventional transmission electron microscopy (TEM) to obtain two-dimensional (2D) projection images of thin sections of virus-infected cells (similar to Figure 1A). The interpretations of such 2D images have intrinsic ambiguities due to overlapping features caused by the projection in the third dimension (Figure 1B). Nonetheless, such thin-section TEM studies have provided valuable insights into the structure of herpesvirus virion and life cycle of herpesvirus infection inside host cells. Our current understandings of structural aspects in herpesvirus life cycle based on these studies includes (reviewed by Arvin et al., 2007) (1) cell-type dependent entry routes (endocytosis or fusion); (2) capsid assembly inside the nucleus; (3) nuclear egress via primary envelopment/de-envelopment process; (4) tegumentation (the capsid acquires tegument protein) in the cytoplasm; (5) secondary envelopment in *trans*-Golgi network (TGN); and (6) egress via exocytosis.

However, a detailed mechanistic description of major events in viral life cycle based on three-dimensional (3D) structures is not available. There are two ways of obtaining 3D structures by TEM, electron tomography (ET) and single-particle analysis by cryoelectron microscopy. Single-particle analysis has been used to determine the 3D structures of highly purified icosahedral capsids of alpha (Trus et al., 1996; Zhou et al., 2000), beta (Chen et al., 1999; Trus et al., 1999), and gamma (Trus et al., 2001; Wu et al., 2000) herpesviruses, in which uniform viral particles are imaged in 2D projections and further classified according to their orientations to generate a 3D model. For pleomorphic or non-repetitive structures, such as the herpesvirus envelope and viral components interacting with host cells (Dai et al., 2008; Grunewald et al., 2003), ET has to be used.

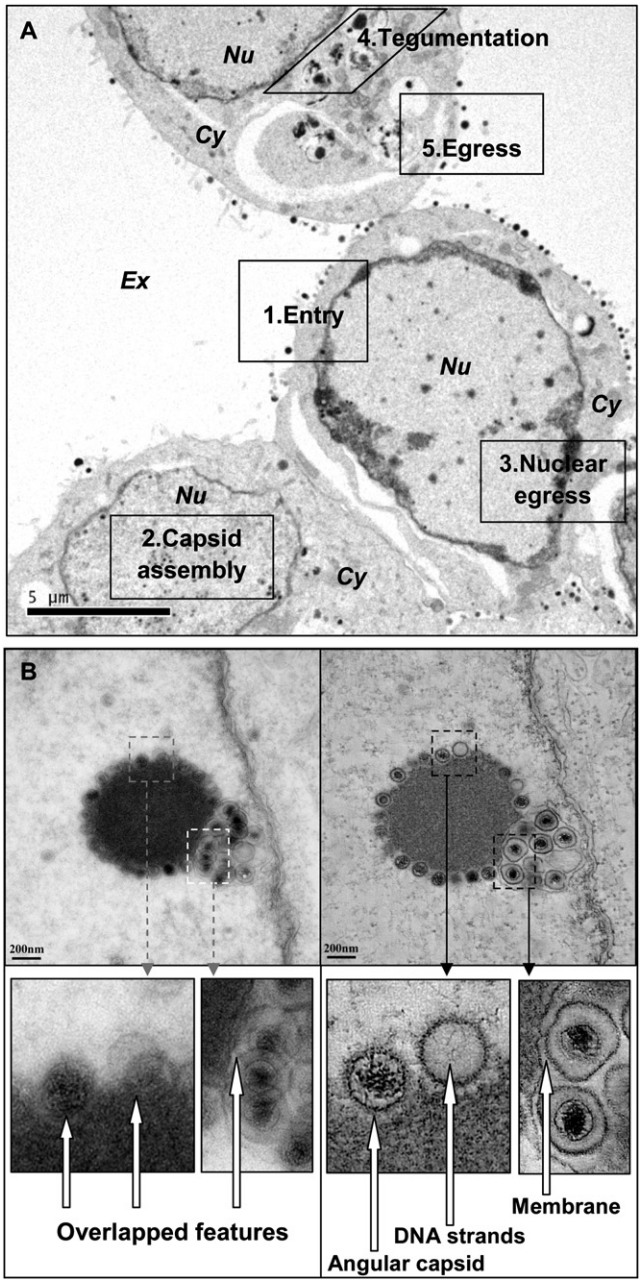

Figure 1. Major Events of Viral Life Cycle and Comparison between 2D TEM Imaging and 3D Visualization by ET

(A) Major events of MHV-68 life cycle illustrated with 2D TEM micrograph.

(B) Comparison between 2D micrograph (left) and digital slice from 3D reconstruction (right). (Note: in all figures of this paper, italic abbreviations used for describing cellular compartments are as follows: *Cy*, cytoplasm; *Nu*, nucleus; *Ve*, vesicle; *Ex*, extracellular space.)

A series of 2D tilt images is recorded at various tilting angles, aligned, and combined to obtain a 3D structure. The 3D reconstruction (tomogram) from a tilt series around a single axis is anisotropically degraded due to the so-called ''missing-wedge problem'' associated with the inherent limit to the range of tilt angles. This can be improved by collecting the dual-axis tilt series (two tilt series of the same object obtained separately around two axes perpendicular to each other) (Mastronarde, 1997; McIntosh et al., 2005). Recently, ET on whole cells embedded in vitreous ice has been used to study HSV-1 entry (Maurer et al., 2008), but this approach is limited to very thin regions of the cell due to the penetration limit of the electron beam (about 300–500 nm). As a result, important events later in the life cycle such as capsid assembly and DNA encapsidation inside the nucleus have not been resolved using this method.

In this study, murine gammaherpesvirus 68 (MHV-68), which is closely related to human gammaherpesviruses (Virgin et al., 1997) and replicates to a high level in many cells, was used as a model system to study the gammaherpesvirus life cycle in host cells. Plastic embedded sectioning and dual-axis ET were combined to achieve direct 3D visualizations of MHV-68 infection, taking advantage of high contrast from the stained sample and improved resolution from dual-axis data set. The data offered the first 3D view of main steps of herpesvirus life cycle and unprecedented insight into the structures and events involved in infection. In particular, this investigation provided novel visualizations of viral DNA injection from the incoming capsid through the nuclear pore, encapsidation of viral DNA into progeny nucleocapsids, and architectures of virus-induced intranuclear inclusion bodies and intranuclear invaginations of both nuclear membranes. The findings not only revealed the structural basis for gammaherpesvirus morphogenesis inside host cells but also illustrated ET as an exciting new avenue for revealing new interactions between virus and host cell.

RESULTS

ET studies of MHV-68-infected cells were performed at various stages of viral infection. Mock-infected and virus-infected fibroblasts (NIH 3T3) were fixed by glutaraldehyde at different time points post infection (p.i.), sectioned, and visualized in three dimensions. Instead of using ~40–70 nm sections common in conventional thin-section 2D TEM, which inevitably cuts the 100 nm diameter herpesvirus capsid in half and fragments large cellular structures, 200 nm thick sections were used to enable observations of complete capsid/virion structures, neighboring cellular structures, and therefore virus-host interactions in viral infection. Samples were examined using TEM and features of interest were identified to collect tilt series for 3D construction. In total, 421 single-axis and 63 dual-axis ET data sets were collected. Reconstructed tomograms were further scrutinized to dissect important events in the viral life cycle and selected structures were segmented and colorized in surface rendering for 3D visualization and interpretation.

The major events of the viral life cycle and the cellular compartments where they took place are shown in Figure 1A. A comparison between 3D reconstruction from dual-axis ET and conventional 2D TEM imaging are shown in Figure 1B (an infection-induced intranuclear inclusion body covered by nucleocapsids, see details below): the left panel shows the TEM micrographs and the right panel shows digital slices extracted from the 3D reconstruction by ET. Overlapped features in 2D images (in ultra-thin sections, the overlap of features still exists, although is less severe than shown here) were clearly resolved in the reconstructed tomogram, indicating the advantage of ET. The angular shape of the nucleocapsid and the viral DNA strands

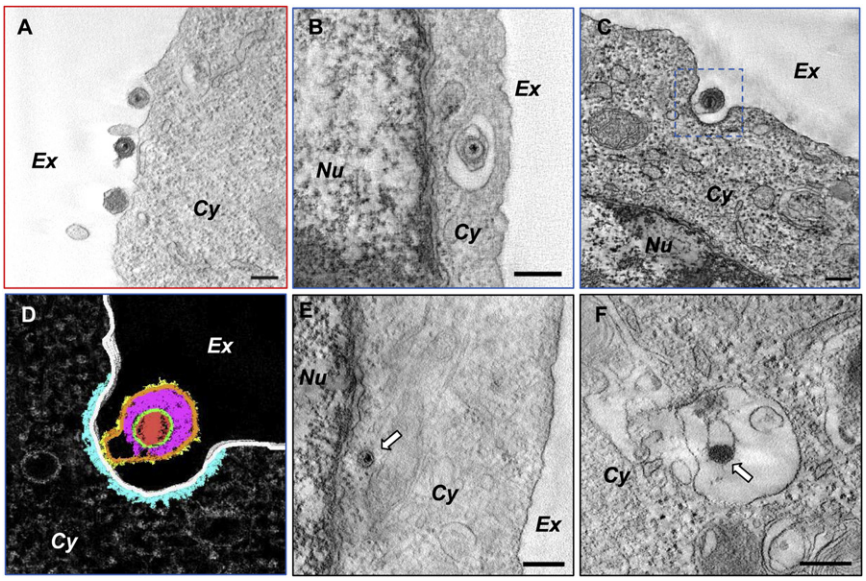

Figure 2. Virus Attachment and Entry

(A–C, E, and F) One nanometer thick digital slices from reconstructed tomograms. (A) A cell incubated with MHV-68 virions at 4°C with viral particles attached; (B–D and F) endocytosis of viral particles; (D) a colorized surface rendering of an 11 nm slab of the feature framed in (B); (E) de-enveloped incoming capsid in the cytoplasm. Color codes in 3D rendering: red, viral DNA; green, capsid; magenta, tegument; orange, envelope; yellow, protrusions on the membrane; light gray, plasma membrane; cyan, membrane coating. Time points (p.i.): (A) 2 hr, (B) 5 min, (E) 20 min, (C, D, and F) 5 hr. Bars: 200 nm. Arrows: (E) enveloped virion; (F) L-particle. (Note: for the following figures, grayscale illustrations are 1 nm think digital slices from reconstructed tomograms, exceptions are otherwise indicated; colorized illustrations, except for Figure 8, are 3D surface renderings of digital slabs from reconstructed tomograms.)

at the beginning of encapsidation visualized in the reconstruction demonstrated the reliability and the resolution of this 3D structural study. Throughout this paper, 1 nm thick digital slices from reconstructed 3D tomograms are shown in grayscale and 3D structures are shown in color (except for Figures 5C and 5F) or movies (as Supplemental Information available online) to illustrate various aspects of 3D viral and host structures.

Virus Attachment and Entry

To visualize initial events of MHV-68 infection, NIH 3T3 cells cultured in 37°C were cooled to 4°C to be inoculated with MHV-68 for 2 hr (MOI = 100). Sections of cells were examined using TEM and areas of interest were further captured by ET for 3D visualization. Reconstructed tomograms revealed that enveloped virus particles and L-particles (virus-like particles comprised of a proteinaceous core without capsid) were frequently located in the vicinity of the plasma membranes. A representative tomogram is shown in Figure 2A. Among all cells examined, no virus particle was detected inside cells, suggesting that viral entry was effectively prevented at 4°C and viral attachment was captured in the tomograms.

Viral entry was observed in cells infected at 37°C and fixed at 5 min, 10 min, 20 min, 1 hr, and 5 hr p.i. (MOI = 100). Enveloped viral particles were present in endosome-like vesicles inside cytoplasm (Figure 2B). Many virus particles were detected within pits characterized by an electron-dense layer coating the inner surface of the plasma membrane (a representative viral particle is shown in Figure 2C), resembling clathrin-mediated endocytosis (Doherty and McMahon, 2009). This is also shown by the 3D colorized surface rendering of an 11 nm thick digital slab extracted from the tomogram (Figure 2D). Virions and L-particles were also found close to uncoated pits (data not shown). De-enveloped capsids were first observed in cells fixed at 20 min p.i. (Figure 2E). L-particles were found in endosomes-like vesicles inside the cells (Figure 2F), indicating that L-particles are entry competent. Notably, no fusion event between the viral envelope and the plasma membrane was seen in any of the cells examined. The results showed that MHV-68 virion enters NIH 3T3 cells via endocytosis under the infection conditions used. This observation is consistent with the previous biological data (Gill et al., 2006).

Viral DNA Injection through Nuclear Pore Complex into Nucleus

After viral entry, incoming capsids with or without DNA were found at peripheral regions of the nucleus, usually close to nuclear pores. Capsids with viral DNA inside were typically present at larger distances than empty capsids from NPCs. Empty capsids were regularly observed docking in the immediate vicinity of nuclear pores and the absence of highly electron-dense cores (DNA density) suggests that the injections of viral DNA from these particles were completed (Figures 3A and 3B). In all tomograms from samples fixed between 20 min and 24 hr p.i., 43 capsids in total were found close to nuclear pores in the cytoplasm. Among them, 26 empty capsids were all approximately 40 nm from NPCs and 15 capsids with viral DNA inside were all more than 80 nm from NPCs. Interestingly, two capsids with only residual densities of DNA strands both inside and outside of capsids (Figures 3C–3F), which we assumed to be in the process of viral DNA injection, were also at about a 40 nm distance from the NPC. The DNA was identified based on its high density and characteristic continuous fibril shape of 2–5 nm in diameter, which is consistent with the diameter of the uranyl acetate-stained DNA, 2.5–4.0 nm, reported in an SEM study (Inaga et al., 1991). The results suggest the viral DNA injection occurs within a more restricted distance from the NPC.

A 3D close-up of the capsid-NPC interaction provided details of the in vivo viral DNA injection process in herpesvirus infection. A capsid juxtaposed to a nuclear pore with one vertex facing the NPC is shown in Figures 3C–3F. In three 1 nm thick digital slices from different positions in z direction, filaments emanating from the NPC were visible (Figure 3D) and the viral DNA releasing from the vertex through the NPC was resolved

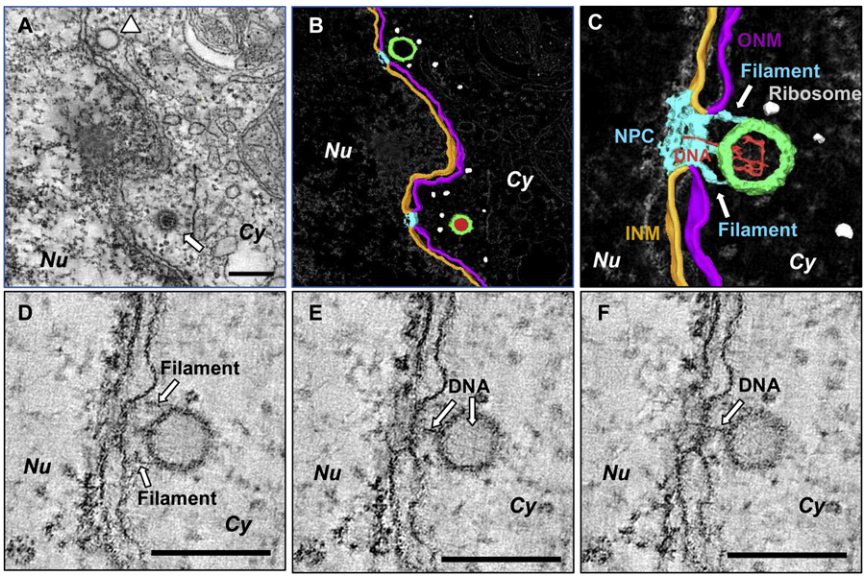

Figure 3. Capsids Docking at Nuclear Pore and Viral DNA Injection

(A) Incoming capsids close to nuclear pores: one empty capsid docked at a nuclear pore and a capsid with viral DNA inside was located about 200 nm away from another nuclear pore. Arrow, capsids with DNA core; arrowhead, capsid without DNA.

(B) An eleven nanometer thick slab of the tomogram shown in (A).

(C) Three-dimensional view of capsid docking at NPC and viral DNA injection (15 nm thick slab).

(D–F) sections from different positions of z dimension from the 3D volume shown in (C). Filaments emanating from the NPC were indicated by arrows in (D) and viral DNA was indicated by arrows in (E) and (F). Color codes in 3D rendering: red, viral DNA; green, capsid; light gray, ribosomes; orange, INM; magenta, ONM; cyan, NPC. Time points (p.i.): (A and B) 5 hr; (C–F) 24 hr. Bars: 200 nm.

(Figures 3E and 3F). A colorized surface rendering (Figure 3C) and a supplemental video (Movie S1) of the same tomogram illustrates this event in three dimensions.

Filaments emanating from the NPC were observed interacting with all 28 capsids (26 empty and 2 with partial viral DNA), which were about 40 nm from the NPC with one vertex facing the NPC. Therefore, the incoming capsid docked at the nuclear pore possibly through interactions between filaments emanating from the NPC and the capsid; and viral DNA was injected from one vertex (presumably, the "portal") into the nucleus through the NPC. This observation resembled the in vitro genome uncoating of HSV-1 capsids following the treatment with trypsin or heating, when the DNA is released as a single double helix at one vertex presumed to be the portal (Newcomb et al., 2007).

Assembly of Nucleocapsids and Encapsidation of Viral Genome

After viral DNA injection, DNA replication takes place, resulting in the appearance of electron-translucent regions inside the nucleus (Figure 4A) where progeny nucleocapsids (Figures 4B and 4C) were usually observed. We also observed incomplete double-layered spheres with particle radius similar to that of complete capsids (Figure 4D) and single-layered spheres with radius similar to that of the scaffolding core (Figure 4E). However, the observation of these particles is rare (only in two tomograms), suggesting that these structures are possible, transient intermediates of capsid assembly.

The use of dual-axis ET improved the resolving power for filamentous structures and allowed us to identify herpesvirus DNA (based on its density, continuous fibril shape, and diameter of 2–5 nm as mentioned above) in the process of being packaged into nascent capsids. Capsids at different stages of DNA encapsidation were detected throughout infected nuclei of cells fixed at 12 hr p.i. (MOI = 50), 24 hr p.i. (MOI = 5), and 36 hr p.i. (MOI = 1). After carefully examining about 200 nucleocapsids, we classified them into six groups and a representative capsid from each group was presented in both 1 nm thick digital slice and 3D surface-rendered illustration (Figures 4F–4Q). A sphere of scaffolding protein existed inside the freshly assembled capsid (pro-capsid) (Figures 4F and 4I) in accordance with previous studies (Newcomb et al., 1996; Tatman et al., 1994). The capsid encapsidating DNA appeared to be more spherical in shape (compare Figures 4G and 4N; also see Figure 1B). Based on the amount of DNA and the presence or absence of scaffolding protein inside the capsids, we sorted the six groups of capsids and proposed two possible DNA encapsidation mechanisms: DNA encapsidation could take place in both capsids without scaffolding protein density (Figures 4G, 4H, 4J, and 4K) and capsids with deformed scaffolding protein (Figures 4L, 4M, 4O, and 4P).

In the former case (without scaffold), the viral genome entered the capsid from a vertex (the putative portal) and started filling in a random pattern (Figures 4G and 4J). As the process went on, more DNA entered and the DNA strand started to line the interior surface of the capsid in circles organized around the "portal" axis (Figures 4H and 4K). A section through the axis of the "portal," shown in Figure 4K, revealed dotted densities decorating the internal surface of the capsid, which we interpreted as cross-sectioned DNA strands. In the latter case (with scaffold), deformed scaffolding protein was observed inside the capsid as an elongated sphere (Figures 4L and 4O). Circularly organized DNA was found inside the capsids with less electron-dense cylindrical shapes in the middle (Figures 4M and 4P). The circular strands of DNA were arranged coaxially with the cylinders that were usually hollow in the middle. In light of the scaffolding protein observed in Figures 4L and 4O, we attribute the cylinder density to deformed scaffolding core possibly immediately after the cleavage of its link to the major capsid protein by the viral protease because, to our knowledge, there are no other candidate proteins present in the capsids at this stage. It is noteworthy that at the end of encapsidation, highly electron-dense DNA was organized in the circular pattern described above and no identifiable less-electron dense cylindrical density existed (Figures 4N and 4Q). A video (Movie S2) illustrates 3D structures of these possible intermediate stages of DNA encapsidation.

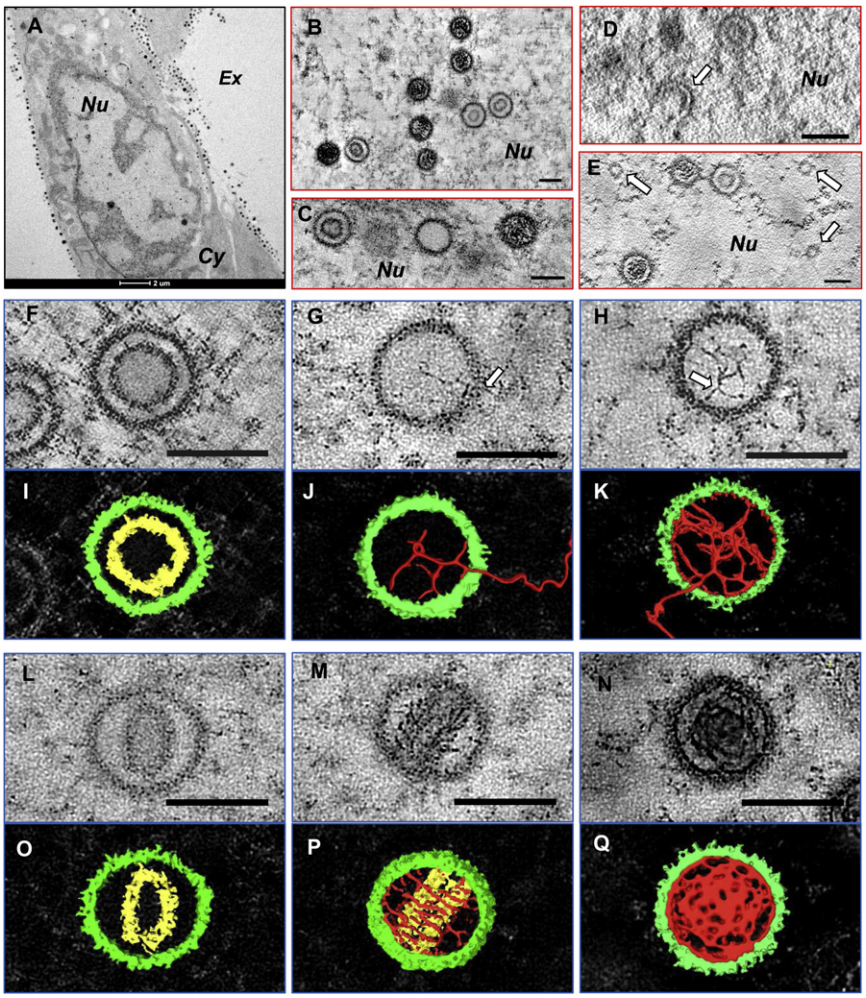

Figure 4. Maturation of Nucleocapsids and Encapsidation of Viral DNA

(A) A TEM micrograph of a MHV-68-infected NIH 3T3 cell.

(B and C) Various kinds of progeny capsids inside nucleus.

(D and E) Possible intermediates in capsid assembly (arrows).

(F–Q) Intermediate stages of viral DNA (arrows) encapsidation process; 3D colored views are rendered from 8 nm thick slabs. Color codes in 3D rendering: red, viral DNA; green, capsid; yellow, scaffolding protein. Time points (p.i.): (A–Q) 24 hr. Bars: (A) 2 μm; others, 100 nm.

These data provide a 3D observation of herpesvirus encapsidation and suggest that viral DNA may enter the capsid either concurrently with or after the removal of scaffolding. At the end of the encapsidation, there is no scaffolding protein left and the viral genome was packaged into a spool with circles of DNA strands organized coaxially with the "portal."

Virus-Induced Intranuclear Inclusion Bodies

In sections of infected cells harvested at 12 hr p.i. (MOI = 50), 24 hr p.i. (MOI = 5), and 36 hr p.i. (MOI = 1), electron-dense spherical inclusion bodies were observed frequently inside infected nuclei (Figures 5A and 5D). The ET reconstructions revealed 3D architectures of these inclusion bodies for the first time and showed that many of them contained nucleocapsids at different stages of maturation at their surfaces (Figures 5B, 5C, 5E, and 5F). The sizes of inclusion bodies and the numbers of capsids covering them varied. A low magnification micrograph of an infected cell (Figure 5A) showed an inclusion body (about 2 μm in diameter) cross-sectioned through the middle with nucleocapsids surrounding it. Another micrograph (Figure 5D) showed the top section of an inclusion body with the capsids present throughout its surface. One nanometer thick digital slices from reconstructed tomograms (Figures 5B and 5E) and shaded surface views of entire sections (Figures 5C and 5F) showed detailed interior architectures and overall morphologies of each inclusion body: both of them are composed of amorphous material as electron dense as the proteinous capsid shell, but less electron dense than the DNA cores in the capsids; holes exist inside the first one (Figure 5B) and fewer capsids cover it; there are no holes in the second inclusion body (Figure 5E), but capsids are observed at a higher packing density and are present in multilayers on its surface.

Primary Envelopment, Invaginations of Nuclear Membrane(s), and Nuclear Egress

Enveloped capsids were found in the perinuclear space (PNS) between two nuclear membranes in cells harvested at 12 hr p.i. (MOI = 50), 24 hr p.i. (MOI = 5), and 36 hr p.i. (MOI = 1) (Figures 6A–6C). After assembly and DNA packaging, capsids budded through the inner nuclear membrane (INM) (Figure 6A), resulting in the formation of enveloped viral capsids in the PNS (Figure 6B). This process is called primary envelopment (reviewed in Mettenleiter, 2002). Interestingly, the region on the INM engulfing the capsid (Figure 6A) and the primary envelope of the capsid (Figure 6B) were thicker and more electron dense than regular regions of the INM. The envelope is smooth without any spike-like protrusions on the surface. The fusion between the primary envelope and the outer nuclear membrane (ONM) was observed, which served as a de-envelopment process and resulted in the release of unenveloped nucleocapsid into the cytoplasm. As shown in Figure 6C, two primary enveloped viral capsids were seen in the PNS and the envelope of the left one appeared to be fusing with the ONM.

We found that MHV-68 infection induced pronounced invaginations of the INM (Figures 6D–6F). Primary enveloped nucleocapsids usually filled the spaces enclosed by the INM invaginations, as shown in Figure 6D. The arrangements of capsids inside the invaginations were either in layers of ordered array pattern if the space were fully filled (Figures 6E and 6F) or in rather random patterns if fewer capsids were enclosed

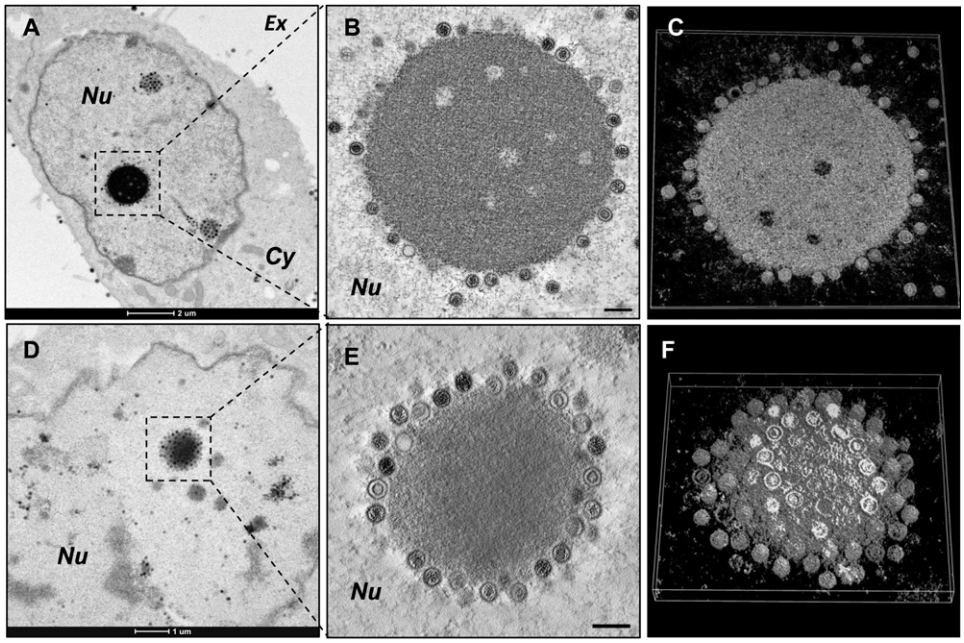

Figure 5. Virus-Induced Nuclear Inclusion Bodies

(A and D) TEM micrographs of infected cells with inclusion bodies.

(B and C) The same inclusion body in (A).

(E and F) The inclusion body in (D).

(C and F) Shaded surface views of entire sections (47 and 135 nm thick) done in chimera. Time points (p.i.): (A–F) 24 hr. Bars: (A) 2 μm; (D) 1 μm; (B and E) 200 nm.

(Figure 6D). In addition, less frequently, double membrane-bounded structures were observed within infected nuclei. As shown in Figures 6G and 6H, enveloped capsids were seen in the lumen between the two membranes and unenveloped capsids were located in double membrane-bounded regions; ribosomes inside the structures revealed the cytoplasmic origin of the contents enclosed by double membranes. Notably, a NPC-like feature was found on the bounding membranes of the structure showed in Figure 6G. The above observations indicate that those structures are invaginated forms of both nuclear membranes. Another such invagination with two nuclear pores was illustrated in Figure 6I. Three 1 nm thick slices from the top (Figure 6J), middle (Figure 6K), and bottom (Figure 6L) of this structure revealed structural details, such as the pit-like structure formed by invaginated membranes (Figure 6K), the connectivity between the contents of the pit and the cytoplasm (Figure 6K), and ribosomes inside the pit (Figures 6J and 6L). A video demonstrating this double-membrane invagination in three dimensions was provided (Movie S3). Both single and double membrane invaginations were observed either close to the edge (Figures 6D and 6G) or in the interior (Figures 6E, 6F, and 6H) of the nucleus on sectioned samples due to different sectioning orientations. Neither type of invagination was observed in mock infected cells. These observations suggest that nuclear membrane invaginations are induced by viral infection and involved in nuclear egress of progeny capsids.

Tegumentation and Secondary Envelopment in the Cytoplasm

In the cytoplasm of cells harvested at 12 hr p.i. (MOI = 50), 24 hr p.i. (MOI = 5), and 36 hr p.i. (MOI = 1), DNA-containing (i.e., C capsids) and a few empty (i.e., A capsids) capsids were observed inside electron-dense deposits that were attributed to tegument proteins (Figure 7A). The capsids were undergoing the tegumentation process, through which they acquired their tegument proteins (reviewed in Mettenleiter, 2002). This process usually occurred close to Golgi-derived membrane structures (TGNs) of various sizes (Figures 7A and 7B). Tegumented capsids budded into TGNs resulting in complete enveloped virions inside exocytic vesicles (Figures 7A–7C). This process is called secondary envelopment (reviewed in Mettenleiter, 2002). Each exocytic vesicle could package a single (Figure 7B) or multiple (Figure 7C) virions and each virion could contain a single or multiple capsids (Figure 7C). L-particles were also detected in exocytic vesicles (Figure 7D). Spike-like protrusions attributable to glycoproteins were present on bilayer envelopes of all kinds of particles at this stage (Figures 7D–7I).

Notably, the tegument proteins within the virions had two distinctive layers, consistent with previous observations of purified MHV-68 virions (Dai et al., 2008). All virions contained an inner, thin spherical layer surrounding the capsid (Figures 7B–7I); and a variable amount of amorphous, mostly asymmetric outer layer was also observed between the inner tegument layer and the envelope (Figures 7D–7F).

Egress and Extracellular Virions

In MHV-68-infected NIH 3T3 cells harvested at late stages of infection (24 hr p.i., MOI = 5, and 36 hr p.i., MOI = 1), exocytic vesicles containing mature virions were frequently observed in the vicinity of the plasma membrane (Figure 7J), consistent with the notion that other herpesviruses (HSV, PRV, and HCMV) egress through the exocytosis pathway (reviewed in

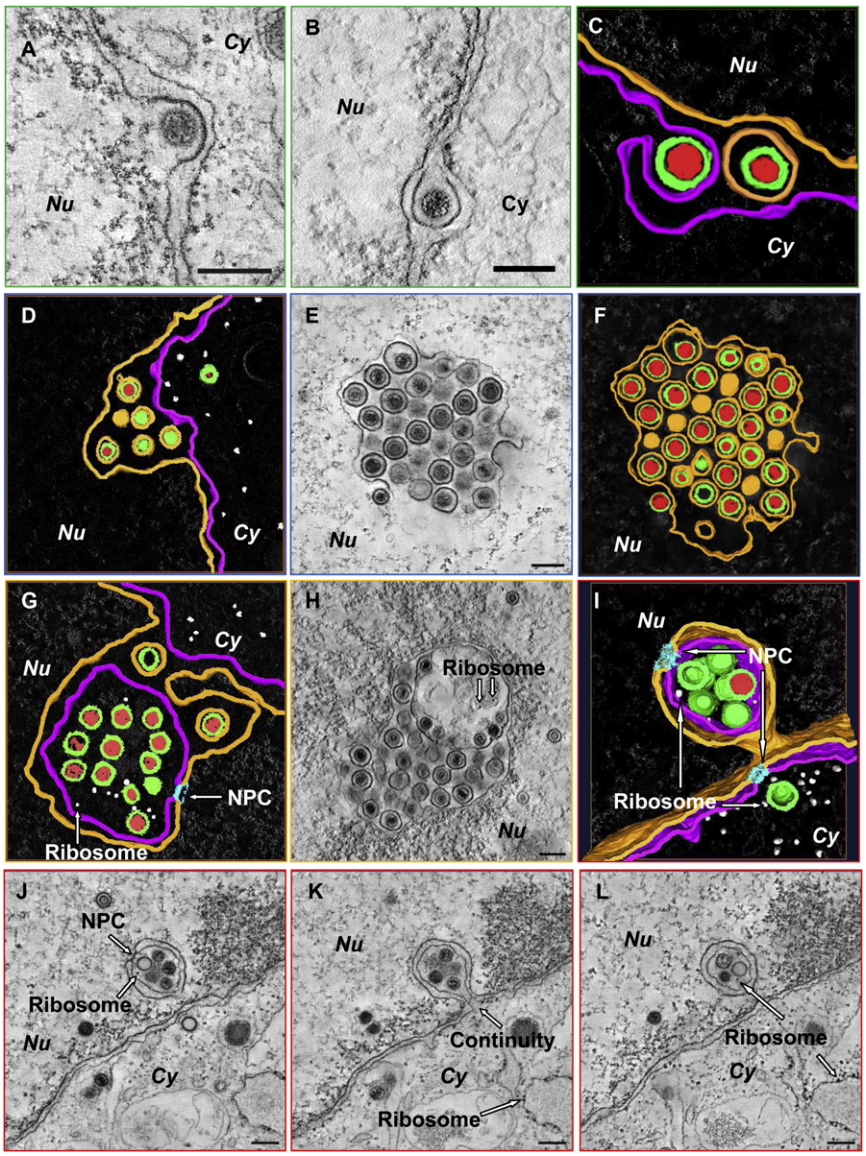

Figure 6. Egress from the Nucleus

(A) A capsid in the budding process on the INM.
(B) A primary enveloped capsid located in the PNS.
(C) An 11 nm thick slab of a fusion event.
(D) An 18 nm thick slab of an INM invagination.
(E) An inner membrane invagination filled with primary enveloped capsids.
(F) A 13 nm thick slab of the invagination shown in (E).
(G) A 7 nm slab of a double-membrane invagination.
(H) A double-membrane invagination.
(I) A 100 nm thick slab of a double membrane invagination.
(J–L) One nanometer digital slices from top, middle, and bottom of the double structure in (I). Color codes in 3D rendering: red, viral DNA; green, capsid; orange, INM or primary envelope; magenta, ONM or primary envelop in fusion; cyan, NPC; light gray, ribosome. Time points (p.i.): (A and C) 36 hr; (B and D–L) 24 hr. Bars: 200 nm.

Mettenleiter, 2004; Mettenleiter et al., 2006). Several kinds of extracellular viral particles, including mature virions (with tegumented DNA-filled capsid) (Figure 7K), replication-defective particles (with tegumented A capsid) (Figure 7L), and L-particles (data not shown), were observed in the peripheral regions of cells. In accordance with the observations of enveloped virions in exocytic vesicles, different amounts of amorphous outer layer tegument proteins were also found within extracellular virions (data not shown). The architecture of the mature extracellular virion was indistinguishable from that of the secondary enveloped virus particle before cellular egress: they were both composed of a bilayer envelope with spikes, a capsid with viral DNA, and tegument densities in between.

DISCUSSION

The results of this 3D structural study of the life cycle of MHV-68 in the host cell led us to a detailed mechanistic model of this gammaherpesvirus that is consistent with observations from previous 2D thin-section EM studies of other herpesviruses (Mettenleiter, 2002, 2004), as illustrated in Figure 8: (1) viral particles enter NIH 3T3 cells via endocytosis; (2) the viral particles are transported in the endosome through the cytoplasm; (3) the incoming capsids dock at the NPC and the viral DNA is injected into the nucleus; (4) after viral DNA replication and protein expression, the nucleocapsids are assembled and the viral DNA is packaged into a spool inside the progeny capsids; (5) intranuclear inclusion bodies are formed; (6) the IMN or both nuclear membranes are invaginated; (7) the nucleocapsids egress from the nucleus via an envelopment and de-envelopment process; (8) the capsids released from the nucleus acquire their tegument in the cytoplasm; (9) the tegumented capsids bud into TNG to acquire the final envelope; (10) the enveloped viral particles are transported in the exocytic vesicles toward the plasma membrane and egress from the host cell via exocytosis. Some details of our model and its relationship with published observations are discussed below.

A note of caution is that ultrastructures obtained by ET in this study could have been affected by the sample preparation method used, such as, fixation, dehydration, embedding, and staining. In this regard, we paid extra caution to interpret only features that are frequently and reproducibly observed in our samples.

Herpesvirus Entry and Viral DNA Injection through NPC

Herpesviruses enter their host cells via different avenues. Studies of HSV-infected cells detect virions fusing with the plasma membrane, as well as virions inside membrane-bound

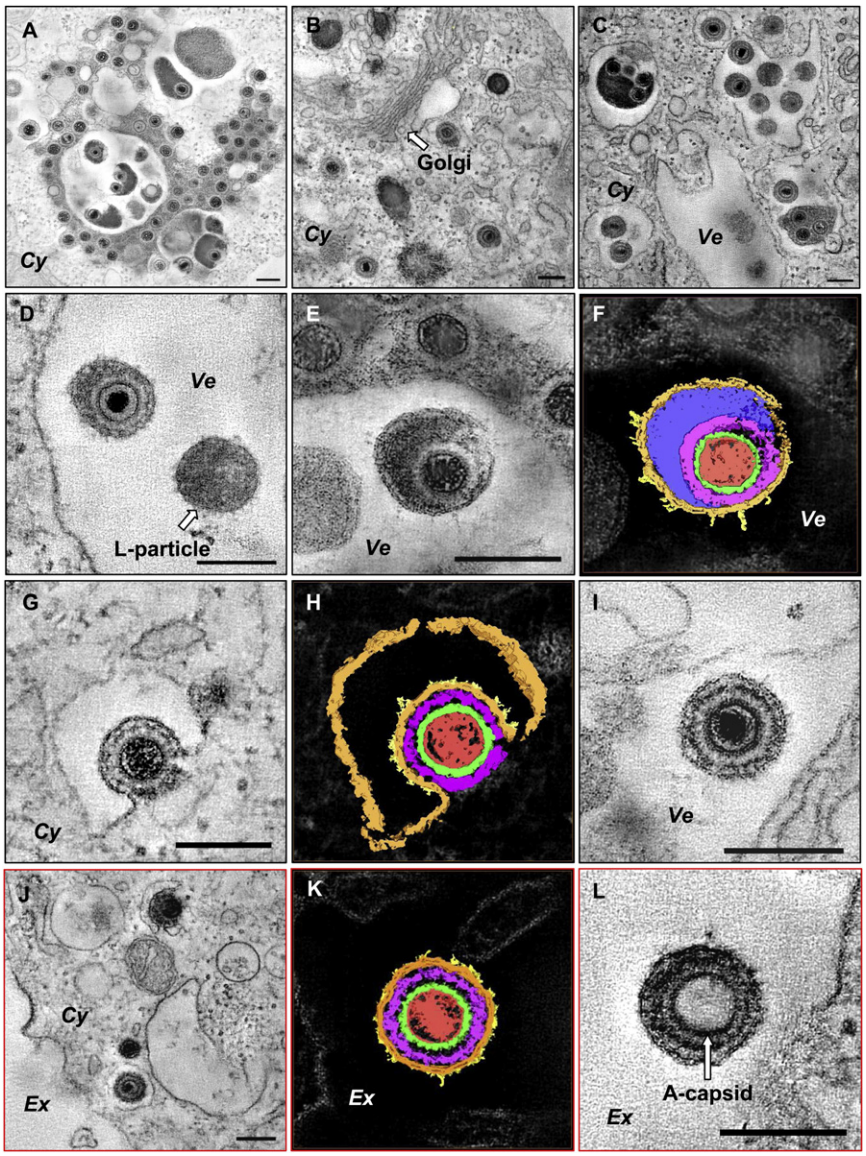

Figure 7. Tegumentation, Secondary Envelopment in Cytoplasm and Extracellular Viral Particles

(A) Capsids were undergoing tegumentation process in bulk accumulations of tegument proteins in the cytoplasm.

(B and C) Secondary envelopment in TGNs.

(D) A virion and a L-particle in an exocytic vesicle.

(E and F) A secondary enveloped particle with large amount of outer layer tegument proteins.

(G and H) Tegumentation and secondary envelopment of a capsid.

(I) A mature virion inside the TGN with spike-like protrusions on the bilayer surface.

(J) An exocytic vesicle containing a mature virion in the vicinity of the plasma membrane.

(K) An extracellular mature virion.

(L) An extracellular enveloped particle with an A capsid inside.

(F, H, and K) Eleven nanometer slabs. Color codes in 3D rendering: red, viral DNA; green, capsid; magenta, inner layer of tegument; blue, outer layer of tegument; orange, envelope; yellow, protrusions of glycoprotein. Time points (p.i.): (B and J) 36 hr; (A, C–I, K, and L) 24 hr. Bars: 200 nm.

vesicles (Nicola et al., 2003); human herpesvirus 6 (HHV-6) is found to infect human lymphoid T cells by endocytosis (Cirone et al., 1992); EBV is reported to fuse with lymphoblastoid cell line Raji but be endocytosed into thin-walled non-clathrin-coated vesicles in normal B cells (Miller and Hutt-Fletcher, 1992); clathrin-mediated endocytosis has been reported to be the main route for KSHV to enter the fibroblast (Akula et al., 2003). In this study, MHV-68 was observed to enter the fibroblast via endocytosis. No fusion event between viral envelope and plasma membrane was present in any of the cells examined. Viral particles were then transported inside the endosome through the cytoplasm. Both clathrin-coated and uncoated endocytic pits were detected, engulfing incoming viral particles. Given the cell type-dependent entry pathways reported for other herpesviruses (such as HSV-1 and EBV), further studies are needed to determine the entry pathway of MHV-68 in non-fibroblast cell types.

Shortly after viral entry, input capsids were found docked at the NPCs with one vertex facing the pore, which is consistent with ultrastructural studies of PRV (Granzow et al., 1997) and HSV-1 (Sodeik et al., 1997)-infected cells. Due to the disappearance of the electron-dense DNA core, viral DNA is proposed to be injected in the nucleus through the nuclear pore (Granzow et al., 1997; Sodeik et al., 1997). Although we could not exclude the possibility that some empty capsids might be A capsids from incoming replication-defective particles (as shown in Figure 7L), which is not a concern because this kind of particle constitute only a tiny portion of total viral particles in virus preparations. To our knowledge, no direct visual evidence for the DNA injection process has been reported, which might be due to the overlapping of features caused by the projection in 2D TEM imaging. In this study, dual-axis ET enabled us to look directly at 3D structures in detail resolving features that would otherwise be obscured; the use of thicker sections (200 nm) not only allowed the entire viral capsid to be examined but also increased the applicable thickness/volume of the sample and thus the opportunity to capture cellular events. These combined advantages made it possible to capture the viral DNA injection event for the first time in three dimensions. As presented in these Results, all empty capsids juxtaposed to the NPCs and capsids undergoing viral DNA injection process detected in our tomograms were invariably approximately 40 nm from the luminal spoke rings of the NPCs and all capsids with viral genome inside were more than 80 nm away from the pores. In light of the 35–50 nm interaction range of the cytoplasmic filaments (originated from the cytoplasmic ring) of the NPCs (Beck et al., 2004, 2007; Copeland et al., 2009; Lim et al., 2008), the observed

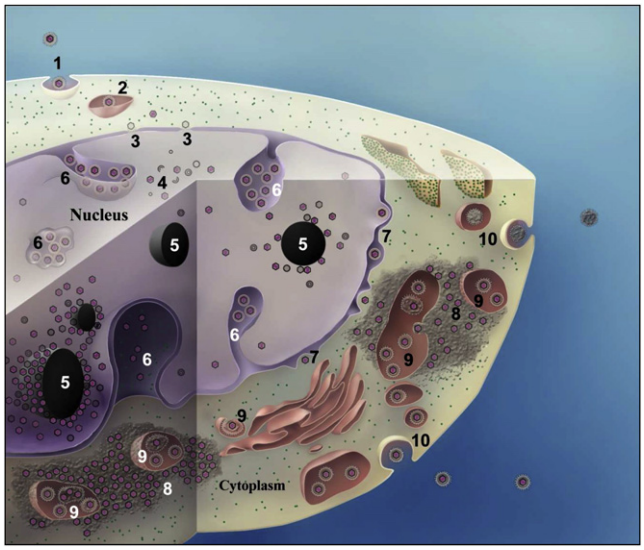

Figure 8. A 3D Illustration of MHV-68 Life Cycle in the Host Cell
An illustration showing entry via endocytosis (1), transportation in endosome (2), viral DNA injection (3), capsid assembly and DNA encapsidation (4), intranuclear inclusion bodies (5), nuclear membrane(s) invaginations (6), egress from nucleus (7), tegumentation (8), secondary envelopment (9), and egress via exocytosis (10). Detailed descriptions were presented in the Discussion section.

results suggested that the release of viral DNA only occurred after the incoming capsids were within the reaching range of the filaments. The binding action of the cytoplasmic filaments to tightly associated tegument (Copeland et al., 2009) on the surface of the input capsids might serve as the trigger for the release of viral DNA. Nucleoporins Nup358 and Nup214 were reported to be involved in this process (Copeland et al., 2009; Pasdeloup et al., 2009).

Encapsidation of Viral DNA

The encapsidation of herpes virus DNA has been visualized by conventional 2D TEM imaging in the form of electron-dense fibers penetrating nucleocapsids. Those fibers are suggested to be higher-order structuring of the DNA (Luetzeler and Heine, 1978; Tralka et al., 1977), which is therefore proposed to be necessary for the efficient packaging of the large genome of herpesvirus (Dargan, 1986). Three-dimensional observations by dual-axis ET in this study showed no such higher-order structure of DNA during MHV-68 encapsidation. Instead the viral DNA was observed entering the capsid as a string. DNA is considered to be the only large biomolecule present inside the mature HSV-1capsid, although a toroid/cylinder structure was suggested as an assembly intermediate (Booy et al., 1991; Brown et al., 2002). In cryoEM studies (Bhella et al., 2000; Booy et al., 1991; Yu et al., 2003), herpesvirus DNA strands are observed to form "fingerprint" patterns inside the virions. However, it remains unclear how the packaging process is carried out. In our 3D in vivo study, proteinaceous cylinders attributed to scaffolding proteins were found during, but not after, DNA encapsidation. In fact, no such cylindrical densities were observed at any stage after the primary envelopment step. These observations are consistent with a proposed model of capsid assembly and maturation, according to which the relative timing between scaffolding cleavage and viral DNA entering is variable among capsids (Yu et al., 2005). Therefore, the capsid with cylindrical protein density and viral DNA existing at the same time is a developmental intermediate if the DNA enters the capsid before the scaffolding protein was removed completely. In contrast, the morphology of viral genome in extracellular virions was observed as highly electron-dense cylinder, which is discussed earlier as the result of specimen preparation procedures, such as fixation, dehydration, staining, etc. (Booy et al., 1991; Puvion-Dutilleul, 1988).

Composition and Possible Roles of Intranuclear Inclusion Bodies

The cytochemical features of herpesvirus-induced intranuclear inclusion bodies have been studied in HSV-1 infection (Besse and Puvion-Dutilleul, 1996; Lopez-Iglesias et al., 1988; Puvion-Dutilleul, 1988). Inclusion bodies are found during the early phase of infection and are characterized as exclusively proteinaceous. Both cellular proteins (nucleolin and fibrillarin) and viral proteins (viral DNase and selected capsid proteins) have been identified in them (Lopez-Iglesias et al., 1988; Puvion-Dutilleul, 1988). In this study, similar inclusion bodies were also detected in MHV-68-infected nuclei. Unlike previous studies, our ET data revealed the 3D architecture of the micrometer-scale inclusion bodies. The frequent presence of nucleocapsids at different stages of maturation at the surfaces of these inclusion bodies and the existence of nucleolar proteins and viral capsid proteins inside suggest that they might play roles in both nuclear structure rearrangement and nucleocapsid assembly.

Nuclear Egress and Invaginations of Nuclear Membrane(s)

The envelopment/de-envelopment process in nuclear egress was reported in all subfamilies of *Herpesviridae* (Mettenleiter et al., 2006). Two viral proteins, pUL31 and pUL34, structurally and functionally conserved in the *Herpesviridae* form a complex and are required to soften and at least partially dissolve the nuclear lamina for the nucleocapsid to achieve the intimate contact with the INM (reviewed by Mettenleiter et al., 2006). The coexpression of these two proteins from PRV has been shown to be sufficient to induce the formation of vesicles from the nuclear membrane (Klupp et al., 2007). Homologs of both proteins in two gammaherpesviruses, EBV (BFLF2 and BFRF1) (Gonnella et al., 2005) and KSHV (ORF69 and ORF67) (Santarelli et al., 2008), have also been reported to be involved in primary envelopment processes. The homologs of these two proteins in MHV68 are ORF69 and ORF67, respectively (Virgin et al., 1997). In this study of MHV-68 infection, INM regions involved in nucleocapsid budding and the primary envelopment of capsids located in the PNS were thicker and had greater electron density compared to regular regions on the INM (Figures 6A and 6B), which might be interpreted as localization of these two proteins. In fact, the interaction between the two proteins was detected in a yeast two-hybrid system (unpublished data). The morphological observations of INM resemble features of HSV infection (Baines et al., 2007); fibers connecting nucleocapsids and INM were also seen (data not shown).

In a study of betaherpesviruses morphogenesis, invaginations of the INM are observed and the structural alteration of the INM has no visible effect on the integrity or shape of the ONM (Buser et al., 2007). In this study, INM invaginations were frequently observed to be filled with primary enveloped capsids. The dramatically dilated INM usually provided increased surface area for budding. In contrast, the non-dilated ONM only provided limited membrane surfaces for fusion/de-envelopment events to take place, which might partially account for the accumulations of enveloped capsids in these invaginations. In addition, invaginations of both nuclear membranes were also discovered in our tomography study. The observed envelopment and de-envelopment events in these structures showed no apparent difference from regular nuclear egress processes, which suggested minimum functional alterations (if any) by architectural modifications of both membranes. Taking advantage of ET, direct 3D evidence for their identity was detected, such as cytoplasm-derived contents, the nuclear pore on invaginated membranes, and, most importantly, the continuity between the invagination and the cytoplasm. The invaginations could have a dynamic nature and a reverse motion of the membranes could possibly restore the invagination and release the capsids "trapped" inside the invagination into the cytoplasm. In HHV-6-infected cells, a structure named "tegusome" is proposed, in which HHV-6 capsids are proposed to acquire tegument (Roffman et al., 1990). Since the tegusome shares all characteristics of the double-membrane invagination as described in this study, they might also share the same identity as invaginated nuclear membranes.

Application of ET in Viral Infections and Structural Study in Cellular Context

Our results demonstrate the value of 3D visualization of complex cellular events using the technology of ET. The major advantage of ET over conventional TEM imaging is its capability of revealing 3D spatial information, thus eliminating ambiguities in identifying cellular structures. The structures revealed in 3D reconstructions can therefore provide direct evidence for interpreting biological processes. For example, in the 2D micrographs of Figure 5D, the inclusion body was only shown as a cluster of nucleocapsids, which could be misleading. In contrast, the 3D reconstructions (Figure 5F) showed the top of a sphere covered with several layers of nucleocapsids, which is the authentic spatial architecture. The use of ET also increases the usable thickness of sample sections (traditionally about 40–70 nm, which is less than the diameter of the nucleocapsid and the NPC) and thus enhances the chances to capture cellular events. For example, in Figure 6K and Movie S3, the channel/connectivity between the cytoplasm and the invaginated region in the nucleus was clearly resolved in the middle of the section. Another example that is made possible only from 3D visualization in this study is the visualization of viral DNA during injection and encapsidation, which cannot be unambiguously interpreted as DNA or traced as continuous strand-like features in conventional thin-section EM. In summary, by applying ET on about 200 nm thick sections, an extensive morphogenetic study of virus-host interaction in MHV-68-infected NIH 3T3 cells was accomplished.

Furthermore, if dynamic events are followed or correlated by integration of ET with other complementary methodologies, such as atomic force microscopy and confocal light microscopy, even more information could be obtained, which is otherwise inaccessible by using any method in isolation. We believe these combined approaches will substantially extend our understanding of fundamental biological questions in the complex cellular context.

EXPERIMENTAL PROCEDURES

Cell Culture and Viral Infection

NIH 3T3 cells were cultured in DMEM with 10% FBS. When 80% confluence was reached, cells were infected with MHV-68 at 4°C for 2 hr or at 37°C for 5 min, 10 min, 20 min, 1 hr, 5 hr (MOI = 100, from 5 min to 5 hr), 12 hr (MOI = 50), 24 hr (MOI = 5), and 36 hr (MOI = 1). The particle to PFU ratio of MHV-68 is about 5-10:1.

Electron Tomography

Cells cultured on 10 cm plates were washed with PBS and fixed for 1 hr in 2% glutaraldehyde in 1× PBS (pH 7.4) on ice. Cell pellets were collected and subjected to osmium post-fixation (1% OsO_4 in PBS) for 1 hr (on ice), 2% uranyl acetate en bloc staining for 1 hr (on ice), followed by dehydration in an ascending ethanol series. The sample was infiltrated and embedded in Spurr's resin and then sectioned about 200 nm using an UCT ultratome (LEICA) with a 35° diamond knife (Diatome). Sections were collected on naked grids (100 mesh, copper) and stained with saturated aqueous uranyl acetate and lead citrate from both sides.

TEM imaging and ET were performed using an FEI Tecnai F20 electron microscope operated at 200 kV. Tilt series were recorded on a TVIPS F415MP 16 megapixel CCD camera at a magnification of 40,600× (for DNA encapsidation, about 12.5 e/Å^2 for each image) or 26,600× (for data other than DNA encapsidation, about 5 e/Å^2 for each image) by tilting the specimen from −70° to 70° with 1° interval using the FEI tomography software Xplore 3D. The defocus was maintained around −2 μm during the data acquisition using the autofocusing function in the Xplore 3D software. Autotracking function was applied after the image was taken at each tilting angle. Dual-axis data sets were collected for selected features by tilting the grid around the x and y axis individually.

Data Processing

Data processing was performed on Linux servers with dual Intel Xeon 5355 (Quad-Core) 2.66 GHz processors and 16 GB memory. For single-axis tilt series, we used the Protomo package (Winkler and Taylor, 2006). Frames in a tilt series were aligned using Protomo's marker-free alignment method by cross-correlation, and 3D reconstructions were computed by weighted back-projection algorithm. For dual-axis tilt series, x and y axis tilt series were reconstructed separately as described above and combined using eTomo in IMOD package (Kremer et al., 1996; Mastronarde, 1997). To merge the reconstructions from x and y axis tilt series, we selected at least five features for matching the tomograms in eTomo's "Tomogram Combination" process.

Segmentation, visualization, snap-shot capture, and video creation were all carried out using Amira 5.2.0 software (Visage Imaging, Inc.). Segmentation was performed based on the density and morphology characteristics of structures of interest using both Amira's automatic (the "magic wand" and "interpolation") and manual (the "brush") tools. Videos showing 3D structures of selected features were produced using Amira's "MovieMaker" module at 24 frames per second in MPG format. The illustration in Figure 8 was prepared in Photoshop CS2 (Adobe).

SUPPLEMENTAL INFORMATION

Supplemental Information includes three movies and can be found with this article online at doi:10.1016/j.str.2009.10.017.

ACKNOWLEDGMENTS

The authors thank W. Dai for her involvement at the initial stage of this project and X. Zhang for graphics illustration. We are grateful to H. Brown and

L. Hughes for critical reading of the manuscript. This project was supported in part by grants from the National Institutes of Health (CA94809/AI069015 to Z.H.Z. and CA091791/DE015752 to R.S.). We acknowledge the use of EM facilities at the Electron Imaging Center for Nanomachines of the University of California, Los Angeles (NIH S10RR23057).

Received: August 8, 2009
Revised: September 3, 2009
Accepted: October 30, 2009
Published: January 12, 2010

REFERENCES

Akula, S.M., Naranatt, P.P., Walia, N.-S., Wang, F.-Z., Fegley, B., and Chandran, B. (2003). Kaposi's sarcoma-associated herpesvirus (human herpesvirus 8) infection of human fibroblast cells occurs through endocytosis. J. Virol. *77*, 7978–7990.

Arvin, A., Campadelli-Fiume, G., Mocarski, E., Moore, P.S., Roizman, B., Whitley, R., and Yamanishi, K. (2007). Human Herpesviruses Biology, Therapy, and Immunoprophylaxis (Cambridge: Cambridge University Press).

Baines, J.D., Hsieh, C.-E., Wills, E., Mannella, C., and Marko, M. (2007). Electron tomography of nascent herpes simplex virus virions. J. Virol. *81*, 2726–2735.

Beck, M., Forster, F., Ecke, M., Plitzko, J.M., Melchior, F., Gerisch, G., Baumeister, W., and Medalia, O. (2004). Nuclear pore complex structure and dynamics revealed by cryoelectron tomography. Science *306*, 1387–1390.

Beck, M., Lucic, V., Forster, F., Baumeister, W., and Medalia, O. (2007). Snapshots of nuclear pore complexes in action captured by cryo-electron tomography. Nature *449*, 611–615.

Besse, S., and Puvion-Dutilleul, F. (1996). Intranuclear retention of ribosomal RNAs in response to herpes simplex virus type 1 infection. J. Cell Sci. *109*, 119–129.

Bhella, D., Rixon, F.J., and Dargan, D.J. (2000). Cryomicroscopy of human cytomegalovirus virions reveals more densely packed genomic DNA than in herpes simplex virus type 1. J. Mol. Biol. *295*, 155–161.

Booy, F.P., Newcomb, W.W., Trus, B.L., Brown, J.C., Baker, T.S., and Steven, A.C. (1991). Liquid-crystalline, phage-like packing of encapsidated DNA in herpes simplex virus. Cell *64*, 1007–1015.

Brown, J.C., McVoy, M.A., and Homa, F.L. (2002). Packaging DNA into Herpesvirus Capsids. In Structure-Function Relationships of Human Pathogenic Viruses (New York: Kluwer Academic/Plenum Publishers), pp. 111–153.

Buser, C., Walther, P., Mertens, T., and Michel, D. (2007). Cytomegalovirus primary envelopment occurs at large infoldings of the inner nuclear membrane. J. Virol. *81*, 3042–3048.

Chen, D.H., Jiang, H., Lee, M., Liu, F., and Zhou, Z.H. (1999). Three-dimensional visualization of tegument/capsid interactions in the intact human cytomegalovirus. Virology *260*, 10–16.

Cirone, M., Zompetta, C., Angeloni, A., Ablashi, D.V., Salahuddin, S.Z., Pavan, A., Torrisi, M.R., Frati, L., and Faggioni, A. (1992). Infection by human herpesvirus 6 (HHV-6) of human lymphoid T cells occurs through an endocytic pathway. AIDS Res. Hum. Retroviruses *8*, 2031–2037.

Copeland, A.M., Newcomb, W.W., and Brown, J.C. (2009). Herpes simplex virus replication: roles of viral proteins and nucleoporins in capsid-nucleus attachment. J. Virol. *83*, 1660–1668.

Dai, W., Jia, Q., Bortz, E., Shah, S., Liu, J., Atanasov, I., Li, X., Taylor, K.A., Sun, R., and Zhou, Z.H. (2008). Unique structures in a tumor herpesvirus revealed by cryo-electron tomography and microscopy. J. Struct. Biol. *161*, 428–438.

Dargan, D.J. (1986). The structure and assembly of herpesviruses. In Electron microscopy of proteins, J.R. Harris and R.W. Horne, eds. (London: Academic Press, Inc. (London), Ltd.), pp. 359–437.

Doherty, G.J., and McMahon, H.T. (2009). Mechanisms of endocytosis. Annu. Rev. Biochem. *78*, 857–902.

Ganem, D. (2007). Kaposi's sarcoma-associated herpesvirus. In Fields Virology, D.M. Knipe and P.M. Howley, eds. (Philadelphia: Lippincott Williams & Wilkins), pp. 2847–2888.

Gill, M.B., Gillet, L., Colaco, S., May, J.S., de Lima, B.D., and Stevenson, P.G. (2006). Murine gammaherpesvirus-68 glycoprotein H-glycoprotein L complex is a major target for neutralizing monoclonal antibodies. J. Gen. Virol. *87*, 1465–1475.

Gonnella, R., Farina, A., Santarelli, R., Raffa, S., Feederle, R., Bei, R., Granato, M., Modesti, A., Frati, L., Delecluse, H.-J., et al. (2005). Characterization and intracellular localization of the Epstein-Barr virus protein BFLF2: interactions with BFRF1 and with the nuclear lamina. J. Virol. *79*, 3713–3727.

Granzow, H., Weiland, F., Jons, A., Klupp, B.G., Karger, A., and Mettenleiter, T.C. (1997). Ultrastructural analysis of the replication cycle of pseudorabies virus in cell culture: a reassessment. J. Virol. *71*, 2072–2082.

Greenspan, J.S., Rabanus, J.P., Petersen, V., and Greenspan, D. (1989). Fine structure of EBV-infected keratinocytes in oral hairy leukoplakia. J. Oral Pathol. Med. *18*, 565–572.

Grunewald, K., Desai, P., Winkler, D.C., Heymann, J.B., Belnap, D.M., Baumeister, W., and Steven, A.C. (2003). Three-dimensional structure of herpes simplex virus from cryo-electron tomography. Science *302*, 1396–1398.

Inaga, S., Osatake, H., and Tanaka, K. (1991). SEM images of DNA double helix and nucleosomes observed by ultrahigh-resolution scanning electron microscopy. J. Electron Microsc. (Tokyo) *40*, 181–186.

Klupp, B.G., Granzow, H., Fuchs, W., Keil, G.M., Finke, S., and Mettenleiter, T.C. (2007). Vesicle formation from the nuclear membrane is induced by coexpression of two conserved herpesvirus proteins. Proc. Natl. Acad. Sci. USA *104*, 7241–7246.

Kremer, J.R., Mastronarde, D.N., and McIntosh, J.R. (1996). Computer visualization of three-dimensional image data using IMOD. J. Struct. Biol. *116*, 71–76.

Lim, R.Y., Aebi, U., and Fahrenkrog, B. (2008). Towards reconciling structure and function in the nuclear pore complex. Histochem. Cell Biol. *129*, 105–116.

Lopez-Iglesias, C., Puvion-Dutilleul, F., Cebrian, J., and Christensen, M.E. (1988). Herpes simplex virus type 1-induced modifications in the distribution of nucleolar B-36 protein. Eur. J. Cell Biol. *46*, 259–269.

Luetzeler, J., and Heine, U. (1978). Nuclear accumulation of filamentous herpes simplex virus DNA late during the replicative cycle. Intervirology *10*, 289–299.

Mastronarde, D.N. (1997). Dual-axis tomography: an approach with alignment methods that preserve resolution. J. Struct. Biol. *120*, 343–352.

Maurer, U.E., Sodeik, B., and Grünewald, K. (2008). Native 3D intermediates of membrane fusion in herpes simplex virus 1 entry. Proc. Natl. Acad. Sci. USA *105*, 10559–10564.

McIntosh, R., Nicastro, D., and Mastronarde, D. (2005). New views of cells in 3D: an introduction to electron tomography. Trends Cell Biol. *15*, 43–51.

Mettenleiter, T.C. (2002). Herpesvirus assembly and egress. J. Virol. *76*, 1537–1547.

Mettenleiter, T.C. (2004). Budding events in herpesvirus morphogenesis. Virus Res. *106*, 167–180.

Mettenleiter, T.C., Klupp, B.G., and Granzow, H. (2006). Herpesvirus assembly: a tale of two membranes. Curr. Opin. Microbiol. *9*, 423–429.

Miller, N., and Hutt-Fletcher, L.M. (1992). Epstein-Barr virus enters B cells and epithelial cells by different routes. J. Virol. *66*, 3409–3414.

Newcomb, W.W., Homa, F.L., Thomsen, D.R., Booy, F.P., Trus, B.L., Steven, A.C., Spencer, J.V., and Brown, J.C. (1996). Assembly of the herpes simplex virus capsid: characterization of intermediates observed during cell-free capsid formation. J. Mol. Biol. *263*, 432–446.

Newcomb, W.W., Booy, F.P., and Brown, J.C. (2007). Uncoating the herpes simplex virus genome. J. Mol. Biol. *370*, 633–642.

Nicola, A.V., McEvoy, A.M., and Straus, S.E. (2003). Roles for endocytosis and low pH in herpes simplex virus entry into HeLa and Chinese hamster ovary cells. J. Virol. *77*, 5324–5332.

Orenstein, J.M., Alkan, S., Blauvelt, A., Jeang, K.T., Weinstein, M.D., Ganem, D., and Herndier, B. (1997). Visualization of human herpesvirus type 8 in Kaposi's sarcoma by light and transmission electron microscopy. AIDS *11*, F35–F45.

Pasdeloup, D., Blondel, D., Isidro, A.L., and Rixon, F.J. (2009). Herpesvirus capsid association with the nuclear pore complex and ciral DNA release involve the nucleoporin CAN/Nup214 and the capsid protein pUL25. J. Virol. *83*, 6610–6623.

Pellett, P.E., and Roizman, B. (2007). The family herpesviridae: a brief introduction. In Fields Virology, D.M. Knipe and P.M. Howley, eds. (Philadelphia: Lippincott Williams & Wilkins), pp. 2479–2499.

Puvion-Dutilleul, F. (1988). Molecular and functional significance of cellular modifications induced by herpes simplex virus infection. Electron Microsc. Rev. *1*, 279–339.

Rickinson, A.B., and Kieff, E. (2007). Epstein-Barr virus. In Fields Virology, D.M. Knipe and P.M. Howley, eds. (Philadelphia: Lippincott Williams & Wilkins), pp. 2656–2700.

Roffman, E., Albert, J.P., Goff, J.P., and Frenkel, N. (1990). Putative site for the acquisition of human herpesvirus 6 virion tegument. J. Virol. *64*, 6308–6313.

Santarelli, R., Farina, A., Granato, M., Gonnella, R., Raffa, S., Leone, L., Bei, R., Modesti, A., Frati, L., Torrisi, M.R., and Faggioni, A. (2008). Identification and characterization of the product encoded by ORF69 of Kaposi's sarcoma-associated herpesvirus. J. Virol. *82*, 4562–4572.

Sodeik, B., Ebersold, M.W., and Helenius, A. (1997). Microtubule-mediated transport of incoming herpes simplex virus 1 capsids to the nucleus. J. Cell Biol. *136*, 1007–1021.

Tatman, J.D., Preston, V.G., Nicholson, P., Elliott, R.M., and Rixon, F.J. (1994). Assembly of herpes simplex virus type 1 capsids using a panel of recombinant baculoviruses. J. Gen. Virol. *75*, 1101–1113.

Tralka, T.S., Costa, J., and Rabson, A. (1977). Electron microscopic study of Herpesvirus saimiri. Virology *80*, 158–165.

Trus, B.L., Booy, F.P., Newcomb, W.W., Brown, J.C., Homa, F.L., Thomsen, D.R., and Steven, A.C. (1996). The herpes simplex virus procapsid: structure, conformational changes upon maturation, and roles of the triplex proteins VP19c and VP23 in assembly. J. Mol. Biol. *263*, 447–462.

Trus, B.L., Gibson, W., Cheng, N., and Steven, A.C. (1999). Capsid structure of simian cytomegalovirus from cryoelectron microscopy: evidence for tegument attachment sites. J. Virol. *73*, 2181–2192.

Trus, B.L., Heymann, J.B., Nealon, K., Cheng, N., Newcomb, W.W., Brown, J.C., Kedes, D.H., and Steven, A.C. (2001). Capsid structure of Kaposi's sarcoma-associated herpesvirus, a gammaherpesvirus, compared to those of an alphaherpesvirus, herpes simplex virus type 1, and a betaherpesvirus, cytomegalovirus. J. Virol. *75*, 2879–2890.

Virgin, H.W., 4th, Latreille, P., Wamsley, P., Hallsworth, K., Weck, K.E., Dal Canto, A.J., and Speck, S.H. (1997). Complete sequence and genomic analysis of murine gammaherpesvirus 68. J. Virol. *71*, 5894–5904.

Winkler, H., and Taylor, K.A. (2006). Accurate marker-free alignment with simultaneous geometry determination and reconstruction of tilt series in electron tomography. Ultramicroscopy *106*, 240–254.

Wu, L., Lo, P., Yu, X., Stoops, J.K., Forghani, B., and Zhou, Z.H. (2000). Three-dimensional structure of the human herpesvirus 8 capsid. J. Virol. *74*, 9646–9654.

Yu, X., O'Connor, C.M., Atanasov, I., Damania, B., Kedes, D.H., and Zhou, Z.H. (2003). Three-dimensional structures of the A, B, and C capsids of rhesus monkey rhadinovirus: insights into gammaherpesvirus capsid assembly, maturation, and DNA packaging. J. Virol. *77*, 13182–13193.

Yu, X.K., Trang, P., Shah, S., Atanasov, I., Kim, Y.-H., Bai, Y., Zhou, Z.H., and Liu, F. (2005). Dissecting human cytomegalovirus gene function and capsid maturation by ribozyme targeting and electron cryomicroscopy. Proc. Natl. Acad. Sci. USA *102*, 7103–7108.

Zhou, Z.H., Dougherty, M., Jakana, J., He, J., Rixon, F.J., and Chiu, W. (2000). Seeing the herpesvirus capsid at 8.5 A. Science *288*, 877–880.

